Programmed mutation of liver fluke granulin using CRISPR/Cas9 attenuates virulence of infection-induced hepatobiliary morbidity

Short title: Attenuated virulence in gene edited parasite

Patpicha Arunsan[1,2,¶], Wannaporn Ittiprasert[2,¶], Michael J. Smout[3,¶], Christina J. Cochran[2], Victoria H. Mann[2], Sujittra Chaiyadet[1], Shannon E. Karinshak[2], Banchob Sripa[4], Neil D. Young[5], Javier Sotillo[3], Alex Loukas[3,*], Paul J. Brindley[2,*] and Thewarach Laha[1,*]

[1]Department of Parasitology, Faculty of Medicine, Khon Kaen University, Khon Kaen 40002, Thailand
[2]Department of Microbiology, Immunology and Tropical Medicine, and Research Center for Neglected Diseases of Poverty, School of Medicine & Health Sciences, George Washington University, Washington, DC 20037, USA
[3]Centre for Biodiscovery and Molecular Development of Therapeutics, Australian Institute of Tropical Health and Medicine, James Cook University, Cairns, QLD 4878, Australia
[4]Department of Pathology, Faculty of Medicine, Khon Kaen University, Khon Kaen 40002, Thailand
[5]Faculty of Veterinary and Agricultural Sciences, The University of Melbourne, Parkville, Victoria 3010 Australia

[¶]These authors contributed equally. [*]These authors contributed equally.

[*]Correspondence: Thewarach Laha, Department of Parasitology, Faculty of Medicine, Khon Kaen University, 123 Mittraparp Highway, Khon Kaen 40002 Thailand. Phone +66 43 348387. E-mail: thewa_la@kku.ac.th

[*] Correspondence: Alex Loukas, Centre for Biodiscovery and Molecular Development of Therapeutics, Queensland Tropical Health Alliance, Australian Institute of Tropical Health and Medicine, James Cook University, Cairns Campus, Cairns, Queensland 4878, Australia; E-mail, alex.loukas@jcu.edu.au

[*]Correspondence: Paul J. Brindley, Department of Microbiology, Immunology and Tropical Medicine, and Research Center for Neglected Diseases of Poverty, School of Medicine & Health Sciences, George Washington University, Washington, DC 20037, USA. E-mail: pbrindley@email.gwu.edu

KEY WORDS: *Opisthorchis viverrini*; liver fluke; genome editing; CRISPR/Cas9; opisthorchiasis; *granulin*; growth factor; cholangiocarcinoma

Abstract

Infections with several flatworm parasites represent group 1 biological carcinogens, *i.e.* definite causes of cancer. Infection with the food-borne liver fluke *Opisthorchis viverrini* causes cholangiocarcinoma (CCA). Whereas the causative agent for most cancers, including CCA in the West, remains obscure, the principal risk factor for CCA in Thailand is opisthorchiasis. We exploited this established link to explore the role of the secreted parasite growth factor termed liver fluke granulin (*Ov*-GRN-1) in pre-malignant lesions of the biliary tract. We targeted the *Ov-grn-1* gene for programmed knockout and investigated gene-edited parasites *in vitro* and in experimentally infected hamsters. Both adult and juvenile stages of the liver fluke were transfected with a plasmid encoding a guide RNA sequence specific for exon 1 of *Ov-grn-1* and the Cas9 nuclease. Deep sequencing of amplicon libraries from genomic DNA from gene-edited parasites exhibited programmed, Cas9-catalyzed mutations within the *Ov-grn-1* locus, and tandem analyses by RT-PCR and western blot revealed rapid depletion of *Ov-grn-1* transcripts and protein. Newly excysted juvenile flukes that had undergone editing of *Ov-grn-1* colonized the biliary tract, grew and developed over a period of 60 days, were active and motile, and induced a clinically relevant pathophysiological tissue phenotype of attenuated biliary hyperplasia and fibrosis in comparison to infection with wild type flukes. This is the first report of gene knock-out using CRISPR/Cas9 in a parasitic flatworm, demonstrating the activity and utility of the process for functional genomics in these pathogens. The striking clinical phenotype highlights the role in virulence that liver fluke growth factors play in biliary tract morbidity during chronic opisthorchiasis.

Introduction

Liver fluke infection caused by species of *Opisthorchis* and *Clonorchis* remains a major public health problem in East Asia and Eastern Europe. *O. viverrini* is endemic in Thailand and Laos, where ~10 million people are infected with the parasite (*1*). There is no stronger link between a human malignancy and a parasitic infection than that between CCA and infection with *O. viverrini* (*2*). In endemic regions such as Northeastern Thailand, infection causes hepatobiliary diseases including cholangitis and periductal fibrosis - a major risk factor for CCA (*3*). The north of Thailand suffers the highest incidence of CCA in the world, often exceeding 80 cases per 100,000 population, and for which up to 20,000 people annually are admitted for surgery. Unfortunately, prognosis for fluke-induced cancer is poor (*1, 4, 5*).

How and why opisthorchiasis induces cholangiocarcinogenesis is likely multi-factorial, including mechanical irritation of the biliary tract during migration and feeding of the liver fluke, inflammatory molecules released by the parasite, and nitrosamines in fermented foods that are a dietary staple in northern Thailand. To survive in the hostile host environment, parasitic helminths produce an assortment of excretory/secretory (ES) products including proteins with diverse roles at the host–parasite interface. This interaction has long been thought but not fully understood to modify cellular homeostasis and contribute to malignant transformation during chronic opisthorchiasis (*6*). Feeding activity of the liver fluke inflicts wounds in the biliary tree, lesions that undergo protracted cycles of repair and re-injury during chronic infection. The liver fluke secretes mediators that accelerate wound resolution in cholangiocytes, an outcome that can be compromised following silencing of expression of *Ov-grn-1* using RNA interference (*7, 8*). We hypothesize that proliferation of biliary epithelial cells induced by *Ov*-GRN-1 is a pivotal factor in establishing a tumorigenic microenvironment in livers of infected individuals.

Progress with development of genetic tools for functional genomic studies with platyhelminth parasites has been limited to date (*9*). The use of clustered regularly interspaced short palindromic repeats (CRISPR) associated with Cas9, an RNA-guided DNA endonuclease enzyme, has revolutionized genome editing in biomedicine, agriculture and biology at large (*10, 11*). Progress with CRISPR/Cas9 in numerous eukaryotes including the nematodes *Caenorhabditis elegans* and *Strongyloides stercoralis* has been described (*11-14*), but this form of gene editing has not been reported for flatworm parasites. Here, we deployed CRISPR/Cas9 to knockout (mutate) the *Ov-grn-1* gene and assess the virulence of gene-edited flukes *in vitro* and *in vivo* in a hamster model of opisthorchiasis.

Results and Discussion

Growth factor secreted by carcinogenic liver mutated by programmed genome ediitng

A construct termed pCas 9-*Ov-grn-1* (Fig. 1a and Supplementary Fig. 1a) was assembled following assessment of the *Ov-grn-1* locus in the annotated genome sequence of *O. viverrini* (*15*). Nucleotide sequences in pCas 9-*Ov-grn-1* were confirmed by Sanger cycle sequencing; pCas 9-*Ov-grn-1* encodes the Cas9 nuclease and a single guide RNA (sgRNA) complementary to a target sequence 5'-GATTCATCTACAAGTGTTGA within exon 1 of *Ov-grn-1*. The predicted programmed cleavage site was predicted to be at three residues upstream of a CGG proto-spacer

138 adjacent motif sequence (PAM) in exon 1 of *Ov-grn-1* (Fig. 1b; Supplementary Fig. 1b). Adult
139 *O. viverrini* flukes recovered from experimentally infected hamsters were subjected *in vitro* to
140 square wave electroporation (*8*) in the presence of pCas 9-*Ov-grn-1* DNA, and thereafter
141 maintained in culture for three weeks. The activity of CRISPR/Cas9 was evaluated by two
142 approaches.
143
144 First, quantitative PCR (qPCR) was employed, which relies on the inefficiency of binding of a
145 primer (here termed OVR-F) overlapping the target genomic sequence of the gRNA, i.e. where
146 mutations are expected to have occurred, compared to the binding efficiency of flanking primers,
147 i.e. outside the mutated region (*16, 17*) (flanking primers termed OUT and OUT-R) (Fig. 1b).
148 Genomic DNA (gDNA) templates were investigated by quantitative PCR to quantify the
149 efficiency of programmed gene-editing at the target locus; the ratio between the OVR-OUT-R
150 products and OUT-F-OUT-R products provided an estimate of the amplification fold-reduction
151 in the sample of CRISPR/Cas9-edited compared to gDNA from control, wild type liver flukes at
152 the target sequence of the sgRNA, i.e. the annealing site for the OVR primer. A reduction in
153 relative fold amplification of 2.7% was detected in gDNA from the Cas9-treated worms (Fig. 1e;
154 Supplementary Fig. 1c).
155
156 Second, to identify and quantify the mutations that arose in the genome of *Ov-grn-1*-edited
157 (termed Δ*Ov-grn-1*) flukes, we used an amplicon-sequencing approach. A targeted (amplicon)
158 sequence library was constructed from genomic DNA from some of the flukes. A 173 bp
159 fragment spanning the predicted double stranded break site of *Ov-grn-1* was amplified from the
160 gDNAs primed with oligonucleotides flanking 1496-1668 nt of *Ov-grn-1.* Adaptors and barcodes
161 were ligated into these amplicon libraries. The MiSeq libraries were undertaken by Illumina
162 MiSeq-based deep sequencing. Insertion-deletion (INDEL)/mutation profiles in the sequence
163 reads were compared in multiple sequence alignment with wild type reference template sequence
164 (1496-1668 nt) of *Ov-grn-1*. Each amplicon was sequenced on the MiSeq Illumina platform and
165 quantified the gene editing frequency by the CRISPResso pipeline (*18, 19*). More than 2 million
166 sequenced reads were aligned against the reference sequence, which predicted the presence of
167 27, 616 non-homologous end joining (NHEJ) reads, specifically 170 reads with insertions
168 (0.6%), 193 reads with deletions (0.7%) and 27,277 reads with substitutions (98.7%). At large,
169 1.25% of the sequenced reads exhibited NHEJ mutations (Fig. 1c). Among these NHEJ reads,
170 there were >100 forms exhibiting mutations that would disrupt the coding sequencing of *Ov-grn-*
171 *1.* Four representatives of the INDEL-bearing traces aligned with the WT allele are presented in
172 Supplementary Fig. 1b. The Illumina sequencing reads are available as GenBank accessions
173 SRR5764463-5764618, at https://www.ncbi.nlm.nih.gov/Traces/study/?acc=SRP110673,
174 Bioproject, www.ncbi.nlm.nih.gov/bioproject/PRJNA385864.
175
176 Effects of gene editing on transcription and protein expression were investigated. Levels of both
177 *Ov-grn-1* mRNA transcripts as determined by RT-PCR and of granulin, as detected by western
178 blot with anti-*Ov*-GRN-1 sera, fell significantly from days 1 and 2 after transfection, respectively
179 ($P \leq 0.0001$; Fig. 1d, e; Supplementary Fig. 1c). Expression levels of two reference genes, the
180 actin transcript (Supplementary Fig. 1c) and the *Ov*-TSP-2 tegument protein (Fig. 1d), were not
181 influenced by the programmed mutation of *Ov-grn-1*.

182 **Mutaion of liver fluke granulin attenuates infection-induced biliary tract morbidity**

183 To investigate whether gene editing of *Ov-grn-1* impacted *in vitro* indicators of pathogenesis, the
184 capacity of ES products from WT, mock-transfected and gene-edited flukes to drive proliferation
185 and scratch wound repair of the H69 human primary cholangiocyte cell line was assessed. ES
186 from WT and mock-transfected adult flukes stimulated cell proliferation and wound closure
187 whereas an equivalent amount of ES products from Δ*Ov-grn-1* flukes resulted in significantly
188 reduced cell proliferation over the six day course of the assay ($P \leq 0.0001$; Fig. 2a, b;
189 Supplementary Fig. 2a, b) and significantly reduced *in vitro* wound closure over 36 hours ($P \leq$
190 0.0001; Fig. 2c; Supplementary Fig. 2c, d), consistent with a reduction in the amount of *Ov*-
191 GRN-1 secreted from the gene-edited liver flukes.

192 Notwithstanding the noteworthy effects observed with gene-edited, adult developmental forms,
193 the metacercaria (MC) (Fig. 3a) is the infective stage of *O. viverrini* for humans. Accordingly,
194 we investigated gene knockout in MC. No effect was apparent on *Ov-grn-1* transcript levels in
195 MC, (Supplementary Fig. 3), suggesting that delivery of the pCas 9-*Ov-grn-1* by electroporation
196 through the MC cyst wall was ineffective. Exposure to bile acids and gastric enzymes results in
197 excystation of *O. viverrini* MC in the duodenum of the infected mammalian host. We mimicked
198 this process *in vitro* using trypsin to release the newly excysted juvenile worms (NEJ; Fig. 3b),
199 after which NEJ were subjected to electroporation with CRISPR/Cas9 constructs as described for
200 adult flukes. Marked depletion of *Ov-grn-1* transcripts ($P < 0.0001$) followed this manipulation
201 (Fig. 3c).
202
203 In parallel, hamsters were infected, using gastric gavage, with 100 Δ*Ov-grn-1* NEJ or WT NEJ
204 immediately after electroporation. At necropsy of the hamsters two to three weeks later, it was
205 clear that Δ*Ov-grn-1* flukes had colonized the bile ducts in similar numbers to WT flukes, and
206 were similarly motile. Strikingly, the infection with Δ*Ov-grn-1* parasites failed to induce the
207 marked hyperplasia of the bile duct epithelia characteristic of infection with WT flukes.
208 Specifically, infection with WT flukes had induced markedly disordered, hyperplasic growth of
209 the epithelium adjacent to the parasites; at day 14, five times more than in uninfected controls (P
210 ≤ 0.0001) (Fig. 3d) whereas infection with the Δ*Ov-grn-1* flukes (Fig. 3e) provoked 11-fold less
211 ($P \leq 0.0001$) biliary hyperplasia than WT fluke infected livers (day 14, 145% thickening
212 compared to uninfected controls; $P \leq 0.01$) (Fig. 3g). Indeed, the bile ducts from hamsters
213 infected with the Δ*Ov-grn-1* flukes generally resembled those of the control, uninfected hamsters
214 (Fig. 3f).

215 To assess long-term survival of Δ*Ov-grn-1* NEJ in hamsters and associated chronic biliary
216 morbidity, hamsters were infected with Δ*Ov-grn-1* and WT NEJ, and adult flukes were
217 recovered and counted from the livers 60 days post-infection. Similar numbers of worms were
218 recovered from both control and gene-edited liver fluke-infected hamsters (Fig. 4a). To assess
219 the impact of infection with Δ*Ov-grn-1* on markers of chronic opisthorchiasis such as biliary
220 fibrosis, liver sections from infected hamsters were stained with Picro-Sirius Red to detect
221 collagen bundles in the biliary tract (Fig. 4b). Minimal deposits of collagen were seen in the
222 periductal regions of the biliary tract of the control, uninfected hamsters whereas hamsters
223 infected with WT flukes had thick bands of collagen surrounding enlarged bile ducts in the
224 vicinity of the flukes. Significantly less collagen (28%) was detected in periductal sites of the
225 biliary tract infected with Δ*Ov-grn-1* flukes ($P < 0.001$) compared to livers of hamsters infected
226 with WT flukes (Fig. 4b, c). To further assess fibrosis in hepatobiliary tract, we stained for
227 smooth muscle actin (ACTA2), an established marker of hepatic fibrosis (*20*), by probing thin

228 tissue sections with anti-ACTA2 antibody. Livers of hamsters infected with WT flukes showed
229 densely packed collagen fibrils that stained for ACTA-2 in periductal regions proximal to the
230 parasites. In contrast, livers from hamsters infected with Δ*Ov-grn-1* flukes displayed an irregular
231 distribution of less dense collagen fibrils with less ACTA2-specific fluorescence (Fig. 4d;
232 Supplementary Fig. 4). The intensity of ACTA2-specific fluorescence was quantified by
233 measuring fluorescence intensity; livers from Δ*Ov-grn-1* fluke-infected hamsters showed 94%
234 reduction (P <0.01) of median fluorescence values relative to controls infected with WT flukes
235 (Fig. 4e).

236 Despite reaching high levels of significance, the data range was high for both markers of
237 collagen deposition assessed. We hypothesized that this was likely due to inconsistencies in the
238 electroporation-mediated delivery of the CRISPR/Cas9 constructs between individual flukes. We
239 therefore collected Δ*Ov-grn-1* and WT flukes from hamster bile ducts 60 days post-infection and
240 assessed *Ov-grn-1* gene expression from individual flukes (Fig. 4f). We then separated flukes
241 into three groups based on *Ov-grn-1* mRNA expression levels: >100% relative to WT average;
242 10-100% relative to WT average; <10% relative to WT average. We pooled genomic DNA from
243 flukes to form the three groups described above and assessed mutation frequencies. In line with
244 the *Ov-grn-1* mRNA expression profiles, Δ*Ov-grn-1* flukes where gene editing appeared to be
245 relatively inefficient (i.e. >100% mRNA expression relative to WT average) had an average
246 mutation frequency of just 0.7%, whereas Δ*Ov-grn-1* flukes where gene editing appeared to be
247 moderately efficient (10-100% mRNA expression relative to WT average) had an average
248 mutation frequency of 3.2%; Δ*Ov-grn-1* flukes where gene editing appeared to be highly
249 efficient (<10% mRNA expression) had an average mutation frequency of 4.6% (Fig. 4f). The
250 combined mutation frequency was 2.7% (Fig. 4f), notably similar to the 2.7% mutation rate
251 detected when Δ*Ov-grn-1* flukes were cultured *in vitro* for 21 days (Fig 1e and Supplementary
252 Fig. 1c).

253 In overview, we describe the first example of successful somatic gene editing of a parasitic
254 flatworm using CRISPR/Cas9. The results revealed that gene editing induced disruption of
255 expression of *Ov-grn-1* in liver flukes, which in turn revealed a pathologically relevant
256 phenotype in the mammalian biliary tract. Following programmed gene editing, the lesion was
257 apparently repaired by non-homologous end joining. The bacterial Type II Cas9 system is active
258 in this liver fluke, and we conjecture that Cas9-catalyzed gene editing will be active in
259 trematodes and parasitic platyhelminths at large. As noted, whereas the causative agent for many
260 cancers, including CCA in the West, remains obscure, the principal risk factor for CCA in
261 Thailand and Laos has long been established - infection with *O. viverrini*. Cas9-based gene
262 editing and the hamster model of human opisthorchiasis utilized herein, including genetic
263 manipulation of the infective NEJ parasite, together provide a facile, functional genomics system
264 to interrogate parasite pathogenicity and carcinogenicity in an informative rodent model of liver
265 fluke infection-induced malignancy.
266
267 **Materials and Methods**
268
269 ***Opisthorchis viverrini* parasite preparation**
270
271 Metacercariae (MC) of *O. viverrini* were isolated from the naturally infected cyprinid fish by
272 pepsin digestion as previously described (*21*). In brief, fishes were minced with an electric

273 blender, and then minced tissues were digested with 0.25% porcine pepsin, 1.5% HCl in 150 mM
274 NaCl at 37ºC in for 2 hours. After tissue digestion, the tissue mixture was filtered sequentially
275 through 1,100, 350, 250, and 140 µm diameter pore size sieves; the final filtrate sedimented by
276 gravity and the aqueous supernatant was discarded. The *O. viverrini* MC enriched-sediment was
277 washed once with 150 mM NaCl (normal saline solution, NSS), and the identity of *O. viverrini*
278 MC confirmed using a stereomicroscope. The *O. viverrini* MCs were stored in NSS at 4ºC until
279 used. The newly excysted-juvenile (NEJs) were prepared from MC in 0.25% trypsin in 1×PBS
280 containing 2× 200U/ml penicillin, 200 µg/ml streptomycin (Gibco) (2× Pen/Strep) for 5 min at
281 RT prior to separate the cyst walls from juvenile parasite by insulin needle (*7, 22*). NEJ were
282 transferred to RPMI medium containing 1% glucose, 2 g/L $NaHCO_3$, 2× Pen/Strep and 1 µM E-
283 64 protease inhibitor (Thermo Fisher Scientific) and maintained at 37ºC, 5% CO_2 for 60 min
284 before use.
285
286 To obtain adult developmental stages of the liver fluke, Syrian golden hamsters (*Mesocricetus*
287 *auratus*) were infected at 6-8 weeks of age with 50 MC per hamster by intragastric tube (*23*).
288 The hamsters were maintained at the Animal Facility of Faculty of Medicine, Khon Kaen
289 University, Khon Kaen, Thailand. Sixty days after infection, hamsters were euthanized and the
290 liver flukes collected, as described (*22, 23*). The study protocol was reviewed and approved by
291 the Animal Ethics Committee of Khon Kaen University. The study adhered to standard
292 guidelines of the Ethics of Animal Experimentation of the National Research Council of
293 Thailand (approval number ACUC-KKU-61/60).
294
295 **Vector and guide RNA targeting exon 1 of *Ov-grn-1***
296
297 To edit the gene *Ov-grn-1* that encodes *O. viverrini* granulin-1 (6287 bp, mRNA GenBank
298 accession FJ436341.1), CRISPR online tools including CRISPR design (http://crispr.mit.edu/)
299 and ChopChop (http://chopchop.cbu.uib.no/) were employed to design a guide RNA (gRNA)
300 targeting exon 1 *Ov-grn-1* gene at nucleotide position 1589-1608,
301 GATTCATCTACAAGTGTTGA (Fig. 1a and 1b). A CRISPR/Cas9 encoding vector encoding
302 the above gRNA under the control of the mammalian U6 promoter and encoding Cas9 (with
303 nuclear localization signal 1 and 2) driven by the CMV promoter was assembled (GeneArt
304 CRISPR Nuclease Vector Kit, Thermo Fisher), and termed pCas-*Ov-grn-1* (Supplementary Fig.
305 1a). *Escherichia coli* TOP-10 competent cells were transformed with pCas-*Ov-grn-1* and vector
306 plasmid recovered from cultures of a positive clone (NucleoBond Xtra Midi, Macherey-Nagel
307 GmbH, Germany). The nucleotide sequence of pCas-*Ov-grn-1* was confirmed by Sanger direct
308 sequencing.
309
310 **Transfection of liver flukes with pCas-*Ov-grn-1***
311
312 Twenty mature flukes were transfected with 10 µg pCas-*Ov-grn-1* pDNA in ~500 µl RPMI-1640
313 (Sigma) by electroporation. The electroporation was performed in 4 mm cuvettes (Bio-Rad) with
314 a single square wave pulse of 125 volts for 20 ms using a Gene Pulser Xcell (Bio-Rad). Flukes
315 were then washed several times with NSS and an additional 5 times with RPMI-1640 containing
316 2× Pen/Strep. Flukes were cultured in RPMI-1640 containing 2× Pen/Step at 37°C in 5% CO_2
317 atmosphere (*7, 24*). Two control groups were included: wild type (WT) mature flukes and
318 'mock' control flukes which were exposed to identical electroporation conditions with RPMI-

319 1640 and 1× Pen/Strep in the absence of plasmid DNA. The adult flukes were observed and
320 collected after 1, 2, 3, 5, 7, 14 and 21 days of culture following pCas-*Ov-grn-1* transfection.
321 RNA and protein was extracted from flukes and *Ov-grn-1* mRNA expression was assessed by
322 RT-qPCR and *Ov*-GRN-1 protein expression was assessed by western blot. Mutations and/or
323 insertions-deletions (INDELs) resulting from CRISPR/Cas were analyzed by CRISPR efficiency
324 estimation (*17, 25*) and MiSeq Next Generation Sequencing (NGS).
325
326 MC and NEJ (750 parasites per cuvette) were subjected to square wave electroporation in the
327 presence of pCas-*Ov-grn-1* pDNA as described above for adult flukes. The parasites were
328 washed as above and cultured in RPMI complete medium (10% FBS, 2× Pen/Strep) at 37°C in
329 5% CO_2 in air. The parasites were collected on days 1, 2, 3 and 5 after transfection and *Ov-grn-1*
330 transcript levels were ascertained by RT-qPCR, as above.
331
332 **Extraction of nucleic acids**
333
334 RNA was extracted from pooled or individual flukes using TRIZOL (Invitrogen) according to
335 the manufacturer's recommendations. Concentration of RNA was estimated by 260 nm by
336 NanoVue spectrophotometer. Genomic DNA from individual or pooled (25 worms) flukes was
337 extracted using the QIAamp DNA Mini Kit (Qiagen, Valencia, CA). The dual RNA and DNA
338 extraction technique was used for some experiments with individual worms using RNAzol®RT
339 (Molecular Research Center, Inc.) and DNAzol (Molecular Research Center, Inc.) (*26, 27*).In
340 brief, each worm was homogenized in RNAzol®RT using a motorized pestle, the DNA and
341 protein from the lysate was precipitated using DNAse-RNAse-free water. The aqueous top
342 solution was transferred into isopropanol to precipitate the RNA. The DNA/protein pellet was
343 resuspended in DNAzol® RT, and DNA extracted as per the manufacturer's instructions.
344 Individual RNA samples were evaluated for *Ov-grn-1* expression. To assess variations in *Ov-*
345 *grn-1* transcript levels, individual flukes were assigned into 3 groups; <10% of *Ov-grn-1*
346 transcript fold change (fc) compared to WT, 10-70% *Ov-grn-1* transcript fc compared to WT,
347 and 100-120% *Ov-grn-1* transcript fc compared to WT. Genomic DNA from individual worms
348 was used to assess CRISPR efficiency and estimate mutation levels (*25, 28*). Estimates of
349 mutation efficiency positively correlated with transcripts levels of Ov-*grn-1* transcript level (Fig.
350 4f). Pooled genomic DNA samples from low to high *Ov-grn-1* transcript levels and high to low
351 percent mutations from experimental groups were prepared for next-generation Illumina
352 sequencing.
353 **Quantitative Real-time PCR**
354
355 Complementary DNA (cDNA) was synthesized from parasite total RNA using an iScript cDNA
356 synthesis kit (Thermo Fisher Scientific) prior to proceeding with quantitative real-time PCR (RT-
357 qPCR). RT-qPCR was performed with biological triplicate samples using a SYBR Green kit
358 (TAKARA Perfect Real-time Kit) according to the manufacturer's recommendation in a Light
359 Cycler 480 II thermal cycler (Roche). Each RT-qPCR reaction consisted of 7.5 µl SYBR Green
360 Master Mix, 0.5 µl (10 µM) each of specific forward and reverse primers for *Ov-grn-1* (Fig. 1b)
361 (forward primer, *Ov-grn-1*-RT-F: 5′-GGGATCGGTTAGTCTAATCTCC and reverse primer,
362 *Ov-grn-1*-RT-R: 5′-GATCATGGGGGTTCACTGTC), amplifying 359 base pairs (bp) of the
363 product (position 7-365 nt of *O. viverrini* granulin-1 mRNA GenBank accession FJ436341.1), 2
364 µl of cDNA and distilled water to a final volume of 15 µl. The thermal cycle was a single

365 initiation cycle at 95°C for 3 min followed by 40 cycles of denaturation at 95°C for 30 sec,
366 annealing at 55°C for 30 sec, extension at 72°C for 45 sec and a final extension at 72°C for 10
367 min. The endogenous actin gene (GenBank accession AY005475) was used as a housekeeping
368 control (*7, 24*) (forward primer, *Ov*-actin-F: 5′-AGCCAACCGAGAGAAGATGA and reverse
369 primer *Ov*-actin-R: 5′-ACCTGACCATCAGGCAGTTC). The *Ov-grn-1* transcript fold change
370 was calculated by 2^(-ΔΔCt) method using *Ov-actin* for normalization (*7, 24, 29*). Means and
371 standard deviations were calculated using Graph Pad Prism software; two-way ANOVA.
372
373 **Rabbit anti-*Ov*-GRN-1 antiserum and immunoblot analysis**
374
375 One milligram of adjuvanted recombinant *Ov*-GRN-1 protein (*30*) was used to subcutaneously
376 inject an outbred New Zealand White rabbit. The rabbit was boosted twice with 500 µg of
377 adjuvanted protein and two weeks after the last booster the rabbit was sacrificed for blood
378 collection via cardiac puncture. The Animal Ethics Committee of Khon Kaen University
379 approved the protocols used for animal experimentation, based on the guidelines of the National
380 Research Council of Thailand for Ethics of Animal Experimentation (ACUC-KKU-61/60). *Ov*-
381 GRN-1 protein levels were determined by western blot using rabbit anti-recombinant *Ov*-GRN-1
382 antiserum. The adult flukes from either WT or Δ*Ov-grn-1* groups were collected individually at
383 days 1, 2, 3, 5, 7, 14 and 21 after electroporation (3 flukes per group). Groups of 3 flukes were
384 homogenized by sonication (Sonics & Materials) in 1× PBS with alternating pulses of 5 sec
385 duration (with 5 sec pause between pulses) for 45 sec at 4°C. The homogenate was centrifuged at
386 13,000 *g* at 4°C for 30 min and the supernatant collected and stored at -20°C. Protein
387 concentration of fluke homogenates was measured using the Bradford assay and homnogenates
388 were electrophoresed on 15% SDS-PAGE gels. Proteins were transblotted onto nitrocellulose
389 membrane using a Mini Trans-Blot Cell (Bio-Rad). Membrane strips containing 2 µg of total
390 protein were washed with 0.5% Tween-20 in PBS (PBST) then blocked for 1 hour with 5%
391 skimmed milk in PBST. Strips were incubated with rabbit anti-*Ov*-GRN-1 serum or pre-
392 immunization serum diluted 1:50 with 1% skimmed milk in PBST and incubated with shaking
393 for 2 h. Strips were washed then incubated for 1 hour with horseradish peroxidase (HRP)-goat
394 anti-rabbit IgG (Invitrogen) (diluted 1:1,000 in antibody buffer). The strips were washed again
395 and color reactions were detected by enhanced chemiluminescence (ECL) substrate (GE
396 Healthcare Life Sciences) and imaged using an Image Quant LAS 4000 mini (GE Healthcare
397 Life Sciences). As a control protein also derived from the tegument of *O. viverrini* flukes, we
398 assessed the protein expression levels of *Ov*-TSP-2 by western blot using a specific antibody
399 raised to the recombinant protein (*31*). Relative protein expression levels from western blots
400 were measured by densitometry using Image J (https://imagej.nih.gov/ij/download.html). Protein
401 expression levels were compared statistically between groups using independent *t*-tests.
402
403 **CRISPR/Cas efficiency and mutation levels estimated by quantitative SYBR green PCR**
404
405 Adult flukes were collected on days 1, 2, 3, 5, 7, 14 and 21 after pCas-*Ov-grn-1* transfection.
406 Each individual fluke DNA was investigated for mutation(s) around the expected double
407 stranded break (DSB) site by using three-primers; 2 forward primers and 1 reverse primer; *Ov-*
408 *grn-1*-OUT-F, *Ov-grn-1*-OVR-F and *Ov-grn-1*-reverse, respectively. The primer pair of *Ov-*
409 *grn-1*-OUT-F and *Ov-grn-1*-reverse was used for amplify the fragment flanking (1496-2312 nt)
410 the DSB, while another primer pair (*Ov-grn-1*-OVR-F and *Ov-grn-1*-reverse) was amplify

411 overlap of DSB site (1599-2312) (Fig. 1b). Both primer pairs exhibited equivalent amplification
412 efficiency with genomic DNA form WT flukes. The OUT and OVR amplicons were 450 and 347
413 bp, respectively, using PCR conditions using 7.5 µl of SYBR Green Master Mix (TAKARA
414 Perfect Real-time Kit), 0.5 µl (0.4 µM) of each primer, 10 ng/µl of gDNA and distilled water to
415 15 µl. The thermal cycles included initiation for one cycle at 95°C for 3 min followed by 40
416 cycles of denaturation at 95°C for 30 s, annealing at 55°C for 30 s, extension at 72°C for 45 s,
417 and a final extension at 72°C for 10 min. The SYBR green signal was read every annealing cycle
418 and reported as threshold cycle (Ct). Efficiency of programmed CRISPR/Cas editing was
419 estimated as the ratio of Ct_{OUT}:Ct_{OVR} from experimental (A) compared with Ct_{OUT}:Ct_{OVR} of
420 control group (B) as described (*17*). The Ct_{OUT}:Ct_{OVR} ratio from control group would equal '1'
421 (CRISPR efficiency = 0) since differences were not seen in Ct value from OUT and OVR
422 primers. By contrast, the OVR primer is anticipated to be less efficient than the OUT primer for
423 the experimental group, and hence the Ct_{OUT}:Ct_{OVR} is less than '1'. Here, we calculated %
424 mutation indirectly by subtraction of the CRISPR/Cas9 efficiency value from '1', as
425 indicated(*17, 32*).
426
427 Average Ct OUT
428 Efficiency (F) = ----------
429 Average Ct OVR
430
431 $F_{\Delta Ov\text{-}grn\text{-}1}$
432 CRISPR/Cas9 efficiency = ----------
433 $F_{Control}$
434 Mutation rate = 100% - CRISPR Cas9 efficiency
435
436 **Illumina-based deep sequencing**
437
438 The MiSeq NGS library was constructed from pooled DNA samples of *Ov-grn-1* gene-edited
439 adult liver flukes at days 14 and 21 post-transfection. The 173 bp amplicon flanking the DSB
440 was amplified from MiSeq-F (position 1496-1514 nt): 5' TTCGAGATTCGGTCAGCCG-3' and
441 MiSeq-R (position 1649-1668 nt): 5'GCACCAACTCGCAACTTACA-3' primers (Fig. 1b). The
442 amplicon was purified (Agencourt AMPure XP beads, Beckman) and ligated with Gene Read
443 Adaptors Set A (Qiagen) and Illumina compatible adaptor(s) and barcode(s) using QIAseq 1-step
444 Amplicon library kit (Qiagen). The library was quantified using a GeneRead Library Quant Kit
445 (Qiagen) with Illumina index/barcode specific primers included in the kit. The concentration of
446 the MiSeq library was read against known standard libraries provided with the Library Quant
447 Kit. NGS was performed at GENEWIZ, South Plainland, NJ). The MiSeq NGS reads were
448 trimmed of index/adaptor and primer out sequences prior to further analysis for programmed
449 mutations by SnapGene software (GSL Biotech LLC) and CRISPResso analysis platform (*18,*
450 *19*) against the target amplicon of the reference (WT) *Ov-grn-1* gene.
451
452 **Illumina-based deep sequencing**
453
454 The MiSeq NGS library was constructed from pooled DNA samples of *Ov-grn-1* gene-edited
455 adult liver flukes at days 14 and 21 post-transfection. The 173 bp amplicon flanking the DSB
456 was amplified from *Ov-grn-1* MiSeq-F (position 1496-1514 nt): 5'

457 TTCGAGATTCGGTCAGCCG-3' and *Ov-grn-1* MiSeq-R (position 1649-1668 nt):
458 5'GCACCAACTCGCAACTTACA-3' primers (Fig. 1b). The amplicon was purified using
459 Agencourt AMPure XP beads (Beckman) and ligated with index/barcoded adapters compatible
460 with the Illumina system using Gene Read Adaptors Set A with the QIAseq 1-step Amplicon
461 library kit (Qiagen). The library was quantified using a GeneRead Library Quant Kit (Qiagen)
462 with Illumina index/barcode specific primers supplied in the kit. The concentration of the MiSeq
463 library was compared with known standard libraries provided with the Library Quant Kit. The
464 MiSeq reads (NGS performed by GENEWIZ, South Plainfield, NJ) were trimmed of
465 index/adaptor and primer out sequences before downstream analysis for programmed mutations
466 by SnapGene software (GSL Biotech LLC) and the CRISPResso platform (*18, 19*) against the
467 target amplicon from the reference WT *Ov-grn-1* gene.
468
469 **Cell proliferation and *in vitro* wound healing assay**
470
471 To evaluate the effect of *Ov-grn-1* gene editing on liver fluke-driven proliferation of human
472 cholangiocytes, motile WT or Δ*Ov-grn-1* adult flukes were co-cultured with cell of the human
473 cholangiocyte cell line H69 in 24-well Trans-well plates (3 wells per groups) (*7*) containing a 4
474 µm pore size membrane separating the upper and lower chambers (Corning).In brief, 15,000 H69
475 cells were seeded into the lower chamber of the plate and cultured with complete medium
476 containing DMEM/F12 supplemented with 1× antibiotic, 10% fetal bovine serum, 25 µg/ml
477 adenine, 5 µg/ml insulin, 1 µg/ml epinephrine, 8.3 µg/ml holo-transferrin, 0.62 µg/ml
478 hydrocortisone, 1.36 µg/ml T3 and 10 ng/ml EGF (*33*) for 24 hours, after which the cells were
479 fasted for 4-6 hours in medium supplemented with only one twentieth of the growth factor
480 content of complete medium. Five viable *O. viverrini* adult flukes that had been transfected (or
481 not) with CRISPR/Cas9 *Ov-grn-1* plasmid in a total of 500 µl of RPMI (or medium alone) were
482 placed into the upper chamber of each well. The number of cells in each well was determined at
483 days 1, 2 and 3 using 1× PrestoBlue cell viability reagent (Invitrogen) (*34*) and added to cells at
484 37°C for up to 1 hour. Cell number was determined at 570 nm and calculated from a standard
485 curve before transforming into relative growth compared to control groups. Cell proliferation
486 assay was carried out in triplicate.
487
488 To assess the effect of *Ov-grn-1* knockout on *in vitro* wound healing, $3x10^5$ H69 cholangiocytes
489 in monolayer were grown in 6-well Trans-well plates with a 4 µm pore size. H69 cells were
490 cultured in complete media for 2 days at 37°C then transferred to incomplete media overnight.
491 Monolayers in each well were scratched using a sterile 200 µl autopipette tip (*7, 8, 35*) and
492 washed with PBS twice to remove disconnected cells or debris. Ten transfected adult or control
493 flukes were added to the upper chamber of the Trans-well plate containing the wounded cell
494 monolayer in the lower chamber. The migration rate of cell wound closure was measured at 0,
495 12, 24 and 36 hours, respectively. Trans-well plates were imaged using an inverted microscope
496 (Nikon) and images of all groups were captured at all-time points quantitatively using Adobe
497 Photoshop CS6. The distances between different sides of the scratch were measured by drawing
498 a line in the middle of the scratch on the captured image (*7, 8, 35, 36*). The analysis of wound
499 healing was carried three times.
500
501 **Infection of hamsters with *Ov-grn-1* gene-edited NEJs and assessment of hepatobiliary**
502 **histopathology**

503
504 Thirty male Syrian golden hamsters, 6-8 weeks of age, were obtained from the Animal Unit,
505 Faculties of Medicine, Khon Kaen University (approval number ACUC-KKU-61/60). The
506 hamsters were randomly divided into three groups of 10 per group: uninfected control, infected
507 with WT flukes and infected with Δ*Ov-grn-1* flukes. Each hamster was infected with 100 active
508 NEJs through intragastric intubation; the uninfected control group was fed normal saline solution
509 instead of NEJ (*23*). Hamsters (5 animals per cage) were contained under conventional
510 conditions and fed a stock diet (C.P. Ltd., Thailand) and water *ad libitum* until they were
511 euthanized (*23*). Following euthanasia, five hamsters from each group were necropsied for
512 histopathological assessment of the hepatobiliary tract at day 14 and at day 60 post-infection
513 (*23*). The hamsters were euthanized by overdose of anesthesia with diethyl ether. Subsequently,
514 blood was obtained by cardiac puncture and the livers were removed. Fluke numbers were
515 counted from two livers of both, WT and Δ*Ov-grn-1* groups at day 60 after infection of hamsters
516 and compared with unpaired two-tailed *t*-test. The left and right lobes of the liver from five
517 hamsters were dissected, cross-sectioned and each lobe was divided into three parts. The liver
518 fragments were fixed in 10% buffered formalin and stored overnight at 4°C before processing.
519 Formalin-fixed liver was dehydrated through an ethanol series (70, 95 and 100%), cleared in
520 xylene and embedded in paraffin. Paraffin embedded sections of 4 µm thickness, cut by
521 microtome, were stained with hematoxylin and eosin (H&E) or Picro-Sirius Red, or probed with
522 anti-ACTA2 antibodies, and analyzed for pathologic changes (below).
523
524 **Biliary hyperplasia**
525
526 H&E staining was used to assess pathological changes. The sections were deparaffinized in
527 100% xylene, rehydrated with descending series of alcohol, stained with H&E for 5 min,
528 dehydrated with an ascending series of alcohol, cleared with 100% xylene, mounted on a slide
529 with permount media, and slides were dried at 37°C overnight and photographed under light
530 microscopy. Images (200×) from H&E stained liver sections from 5 untreated control hamsters
531 or 5 hamsters per treatment group (WT and Δ*Ov-grn-1* groups) were assessed. Thickness (width)
532 of the bile duct epithelium from each thin liver section was measured with ImageJ at eight
533 equidistant positions around the bile duct. To compensate for outliers the median width for each
534 bile duct was used for graphing and analysis. The two-way ANOVA Holm-Sidak multiple
535 comparison test was used to compare each group at each time point.
536
537 **Fibrosis**
538
539 Two stains were used separately to assess biliary fibrosis. First, sections were stained with Picro-
540 Sirius Red (Abcam, Cambridge Science Park, UK). Sufficient Picro-Sirius Red solution was
541 applied to completely cover the tissue sections on the slide, the stained slide was incubated at
542 ambient temperature for 60 min, rinsed in two changes of acetic acid solution, and dehydrated
543 through two changes of absolute ethanol. Slides were cleared with 100% xylene, mounted in Per-
544 mount, dried at 37°C overnight, and examined and photographed by light microscopy to
545 document collagen surrounding the bile ducts. ImageJ was used to auto-color balance the images
546 using the macro written by Vytas Bindokas; Oct 2006, Univ. of Chicago
547 (https://digital.bsd.uchicago.edu/docs/imagej_macros/_graybalancetoROI.txt) followed by
548 application of the MRI fibrosis tool to determine percentage area of red-stained fibrosis at default

549 settings (red 1: 0.148, green 1: 0.772, blue 1: 0.618, red 2: 0.462, green 2: 0.602, blue 2: 0.651,
550 red 3: 0.187, green 3: 0.523, blue 3: 0.831) (*37*). Twenty discrete images (200×) stained with
551 Picro-Sirius Red from each animal (five hamsters per treatment group) were assessed (in total,
552 100 images per group). Kruskal-Wallis with Dunn's multiple comparison test was used to
553 compare the findings due to the range of data points among the groups.
554
555 Fibrosis was also assessed via levels of smooth muscle alpha-actin (ACTA2). Liver sections
556 from hamsters at day 60 post-infection were deparaffinized three times with 100% xylene, 5 min
557 each. Sections were rehydrated with ascending series of ethanol; 100%, 3 times, 3 min each,
558 95% 3 times, 3 min each, 70% for 3 min, followed by thorough washing in tap water for 5 min,
559 distilled water for 5 min, and PBS for 5 min. Thereafter, slides were incubated in citrate buffer
560 pH 6.0 (citric acid (anhydrous) 1.92 g and Tween 20 0.5 ml in total volume of DW 1000 ml) at
561 110°C for 5 min, allowed to cool for 20 min, and then washed in PBS 3 times, 5 min each.
562 Sections were then blocked with 5% bovine serum albumen (BSA) for 30 min in a humidified
563 chamber and washed in PBS 3 times, 3 min each with occasional shaking. The slides were
564 probed with Alexa Fluor 594 –labeled anti-ACTA2 antibody (Abcam) diluted 1:200 in 1% BSA
565 in PBST, 18 hours at 4°C in a humidified atmosphere. Lastly, slides were washed in PBS 3
566 times, 3 min each with occasional shaking, mounted in glycerol diluted 1:4 with PBS and
567 examined under bright and fluorescence light (Zeiss Axio Observer, with AxioVision SE64 Rel.
568 4.9.1 software, Jena, Germany). Images with a bile duct containing a fluke were selected and
569 ImageJ was used to manually select a narrow strip surrounding the bile duct epithelial layer that
570 excluded potential blood vessels (any enclosed curved oval-like shape). Three liver regions not
571 including the bile duct or blood vessels were manually selected for background fluorescence
572 measurements, each comprising 5-10% of the image. The fluorescence intensity of the bile duct
573 epithelial strip was measured and blanked against the average of the three background regions
574 and reported as average intensity per cm^2 at 300 PPI (pixels per inch). A total of 25-30 distinct
575 bile duct images per group (3 animals) were assessed. Zero values from the uninfected group
576 were deemed to have a value of 1 to allow a log axis. The groups were compared with one-way
577 ANOVA with Holm-Sidak multiple comparison test.
578
579 **ACKNOWLEDGMENTS**
580
581 We thank Suwit Balthaisong for technical assistance. This study was supported by the Thailand
582 Research Fund through the Royal Golden Jubilee PhD Program (grant no. PHD/0111/2557 to PA
583 and TL), the National Cancer Institute (NCI), US National Institutes of Health (NIH) award
584 R01CA164719 (AL, TL, PJB,) and the National Health and Medical Research Council (NHMRC
585 award APP1085309 to AL, JS and TL, and senior principal research fellowship APP1117504 to
586 AL). The content is solely the responsibility of the authors and does not necessarily represent the
587 official views of the NIAID, NCI, NIH or NHMRC. These studies were supported in part by
588 Wellcome Trust Strategic Award number 107475/Z/15/Z (Karl F. Hoffmann, principal
589 investigator; PJB, co-investigator).
590
591 **AUTHOR CONTRIBUTIONS**
592
593 T. Laha, P.J. Brindley, W. Ittiprasert , P. Arunsan, N. D. Young, A. Loukas, J. Sotillo, M. Smout,
594 S. Chaiyadet, C. Cochran, and V. Mann conceived and designed the research; P. Arunsan, M.

Smout, J. Sotillo, S. Karinshak and W. Ittiprasert performed the research; P. Arunsan and M. Smout recorded the findings ; T. Laha, P.J. Brindley, M. Smout and W. Ittiprasert contributed reagents and analytic tools; T. Laha, P.J. Brindley, M. Smout, J. Sotillo and P. Arunsan completed the experiments; T. Laha, P. Arunsan, W. Ittiprasert, J. Sotillo and M. Smout analyzed data; T. Laha, P. Arunsan, W. Ittiprasert, M. Smout, A. Loukas and P.J. Brindley prepared figures and wrote the paper.

The authors declare no competing interests.

641
642 **(*6*)Figure legends**
643
644 **Figure 1 CRISPR/Cas9-mediated gene editing strategy to knock-out *Ov-grn-1* in adult**
645 ***Opisthorchis viverrini* liver flukes. a**, Schematic depiction of *Ov-grn-1* gene with CRISPR/Cas9
646 target site in first exon marked with green arrow. **b**, The exon1, 2 and 3 location of *Ov-grn-1*
647 gene, size of 6,267 bp and gRNA targeting exon1: gRNA sequence is blue color and PAM is red
648 in bracket. Primer pairs were used to detect mRNA expression levels by using RT-qPCR assay
649 (*Ov-grn-1* RT- forward or RT-F and *Ov-grn-1* RT-reverse or RT-R), Tri-primers were used to
650 detect the % relative fold amplicon or mutations (outside-forward or OUT-F, overlap-forward or
651 OVR-F and reverse primer or OUT/OVR-R) and MiSeq forward and reverse (MiSeq-F and
652 MiSeq-R) primers were used to prepare the NGS amplicon. **c**, CRISPR/Cas9-induced adult
653 fluke genomic insertion (red bars) and deletion (black bars) mutations (INDELs) detected in the
654 *Ov-grn-1* gene; CRISPR target site is denoted by the green arrow. Average mutation length is
655 plotted against *Ov-grn-1* gene amplicon position in base pairs (bp). **d**, Somatic tissues of
656 individual adult worms (in triplicate per time per group) were solubilized, electrophoresed in
657 SDS-PAGE gels, transferred to nitrocellulose membrane and probed with anti-*Ov*-GRN-1 rabbit
658 antibody. WT: wild type control fluke tissues; D1-21: Δ*Ov-grn-1* fluke tissues sampled the arrow
659 highlighting the ~9 kDa *Ov*-GRN-1 band at different days post-transfection and Δ*Ov-grn-1*
660 flukes show similar *Ov*-TSP-2 protein (control antibody) expression levels. D1-21 = protein
661 products from flukes day 1-21 post Δ*Ov-grn-1* treatment. Western blot panels of probed with
662 anti-*Ov*-TSP-2 rabbit antibody, the arrow highlighting the ~24 kDa *Ov*-TSP-2 band. **e**, Reduced
663 expression of *Ov-grn-1* mRNA and *Ov*-GRN-1 protein after transfection of adult flukes with *Ov-*
664 *grn-1* CRISPR/Cas9 construct using quantitative real-time PCR (mRNA) and densitometry
665 conversion of Western blot signals (protein). Data are plotted relative to wild type (WT) fluke
666 values (100%) as an average percentage from 3 replicates with SD error bars. **** = $P<0.0001$
667 compared to WT fluke protein (black) or RNA (pink) at each time point with two-way ANOVA
668 Holm-Sidak multiple comparison test.

669 **Figure 2 Δ*Ov-grn-1* adult fluke ES products induce less *in vitro* cell proliferation and**
670 **wound repair. a**, Representative cell proliferation images of H69 immortalized human
671 cholangiocyte cell line co-cultured with flukes in Trans-well plates; mock transfected (top) and
672 Δ*Ov-grn-1* (bottom) groups are shown at day 3. **b**, Reduced cell proliferation induced by *ΔOv-*
673 *grn-1* fluke ES products, as shown in panel a, quantified from days 1-6. Data is plotted as
674 average relative percentage to cells cultured with "no flukes". **c**, Representative image of H69
675 cholangiocyte scratch wound repair when cells were co-cultured in Trans-well plates with flukes.
676 Mock transfected (top) and Δ*Ov-grn-1* (bottom) groups are shown at 0 and 36 h post-scratch
677 wounding. Dotted line shows the edge of the wound. **d**, Scratch wound repair assay quantified
678 from 0 to 36 hours, reveling diminished healing in the Δ*Ov-grn-1* group. Panels **b** and **d**: mean ±
679 SD, three replicates; ****$P<0.0001$ compared to wild type flukes with two-way ANOVA Holm-
680 Sidak multiple comparison test.
681
682 **Figure 3 Δ*Ov-grn-1* newly excysted juveniles can infect hamsters and drive reduced short-**
683 **term pathology.** Images of infective metacercariae (**a**) and newly excysted juvenile flukes
684 (NEJ) (**b**). **c**, *Ov-grn-1* mRNA expression in mock-transfected and Δ*Ov-grn-1* flukes over 5 days
685 as quantified with qPCR and plotted relative to the wild type (WT) untreated group; mean ± SD,
686 three replicates; **** = $P<0.0001$ compared to WT flukes with two-way ANOVA Holm-Sidak

687 multiple comparison test at each time point. **d**, Representative image of 400x magnification of
688 H&E stained thin section from hamster liver at 14 days after infection with WT flukes. **e**,
689 Representative image of H&E stained thin sections showing hamster liver 14 days after infection
690 with Δ*Ov-grn-1* flukes. **f**, Representative image of H&E stained thin section of control,
691 uninfected hamster liver, which shows healthy, organized pavement-like profile of the cells of
692 the biliary epithelium (BE) enclosing the lumen of the bile duct (BD) near a blood vessel (BV)
693 within the liver (L). Infection by WT flukes (panel **d**) revealed thickened, disordered epithelium
694 adjacent to the parasite (*Ov*). Infection with Δ*Ov-grn-1* flukes (panel **e**) revealed a bile duct
695 epithelium more closely resembling the normal, uninfected hamster. **g**, Epithelium
696 width/hyperplasia (green bracket) was quantified using ImageJ and plotted as the mean ± SD of
697 five biological replicates (hamsters). Significant difference were apparent when compared to the
698 uninfected group using the two-way ANOVA with Holm-Sidak multiple comparison test:
699 $^{**}P<0.01$ and $^{****}P<0.0001$, and wild-type compared to Δ*Ov-grn-1*, $^{\#}P<0.05$ and
700 $^{\#\#\#\#}P<0.0001$.
701
702 **Figure 4. Diminished level of fibrosis in hamsters during chronic infection with gene-edited**
703 **Δ*Ov-grn-1* liver flukes.** Panel **a**, Adult fluke numbers were counted from the livers at day 60
704 post-infection and shown as the average and range for two hamsters per group . Fluke counts
705 showed minimal (12%; *ns*) difference between the wild type (WT) and Δ*Ov-grn-1* groups. **b,**
706 Representative images of Sirius red stained hamster liver (L) sections from uninfected animals
707 show minimal collagen fibrosis (fb) deposition, stained red surrounding the blood vessel (BV)
708 and bile ducts (BD) with normal biliary epithelia (BE). Livers from hamsters infected with WT
709 flukes (*Ov*) show heavy collagen deposition with elongated BE cells adjacent to resident flukes. .
710 Δ*Ov-grn-1* fluke infected livers showed substantial collagen deposition compared to uninfected
711 liver sections, yet showed far less than the livers infected with WT flukes. **c**, Liver fibrosis
712 quantified with ImageJ MRI-fibrosis plugin shown as a violin plot. 100 images containing bile
713 ducts from 20 sections (5 animals) per group showing SD as a vertical line with the median
714 indicated by the central black dot. Δ*Ov-grn-1* group showed a 23% reduction in median fibrosis
715 compared to WT group. The width of the "violin-shape" represents measurement frequency.
716 Kruskal-Wallis with Dunn's multiple comparison test used to compare groups. Against
717 uninfected: $^{****}P<0.0001$, and Δ*Ov-grn-1* against WT: ### $P<0.001$. **d**, Representative
718 immunofluorescence/bright field overlay images of liver sections probed with anti-ACTA2
719 antibody with fluorescence intensity shown on a blue/green/red scale. ACTA2 protein is always
720 detected in my fibroblasts surrounding blood vessels, but not near normal bile ducts. When
721 detected near the BE layer it is suggestive of myofibroblast generation as a response to BE
722 damage. The upper panels (Overlay) show a wide view of the liver sections with a boxed region
723 that highlights a section of interest that is magnified in the lower panels (Zoom). Hamster liver
724 sections exhibited intense fluorescence (arteries: red/green, veins: blue/green) surrounding BVs
725 whereas only minimal fluorescence was seen near BD in livers of uninfected hamsters The
726 highlighted magnified (Zoom) panels show WT infected animal livers with weak (blue) but
727 consistent ACTA2 staining surrounding thickened BE layer (inner and outer cell edge marked
728 with orange dotted line) around BDs with WT flukes. Livers from hamsters infected with Δ*Ov-*
729 *grn-1* flukes show weak and irregular ACTA2 staining surrounding BD. **e**, Quantified levels of
730 ACTA2 surrounding BDs from hamster liver sections. Violin plot with reverse log2 Y-axis
731 showing the ACTA2 intensity (per cm^2 at 300 PPI) surrounding BE from 25-30 discrete BD
732 images per group (three hamsters) assessed with ImageJ. Zero values from uninfected group

were deemed to have a value of 1 so that a log axis could be plotted. SD indicated as a line with mean value marked as a central black dot and the violin-shape width representing measurement frequency. ACTA2 staining shows 94% median reduction in Δ*Ov-grn-1* fluke-infected livers compared to WT fluke-infected animals. One-way ANOVA with Holm-Sidak multiple comparison test, ****P<0.0001 compared to uninfected and ##P<0.001 compared to Δ*Ov-grn-1* flukes against WT flukes. **f**, *Ov-grn-1* mRNA expression levels are reduced in Δ*Ov-grn-1* flukes compared to WT flukes. Reverse log10 Y-axis shows the qPCR 2^(-ΔΔCt) results from flukes 60 days after programmed CRISPR/Cas9 gene editing and hamster infection plotted relative to mean value of the WT infection. The WT group showed a broad level of expression; the mean expression level for the Δ*Ov-grn-1* flukes was 19.4% of the WT group; Mann-Whitney nonparametric test, ***P*<0.01. While significantly reduced overall, the Δ*Ov-grn-1* fluke group ranged from no apparent effect to markedly diminished expression of *Ov-grn-1*. Mutation frequency was assessed by assigning the Δ*Ov-grn-1* group of flukes into three sub-groups based on CRISPR/Cas9 mutation frequency. Eight flukes with highly effective CRISPR gene knock-out (Δ*Ov-grn-1*: *Ov-grn-1*<10% expression), seven flukes with modest levels of transcript knock-out (Δ*Ov-grn-1*: 10-70% *Ov-grn-1*) and 10 flukes with little or no effect (Δ*Ov-grn-1*: *Ov-grn-1* 100-120%). The mean mutation frequency amongst the three Δ*Ov-grn-1* sub-groups was 2.7%.

779
780 **Supporting information**
781
782 **Supplementary Figure 1. CRISPR/Cas9 targeting *Ov-grn-1* design and flukes transfection.**
783 **a**, *Ov-grn-1* guide RNA insertion and Cas9 cassette. **b**, The original *Ov-grn-1* sequence with the
784 target (red text) and PAM (blue text) sites highlighted. The dark green arrow indicates the
785 specific CRISPR target site. Deep sequencing is used to determine specific mutations and the
786 four sequences below the original sequence show examples of successfully mutated *Ov-grn-1*
787 genes with variations with red boxed bases highlighted mutations induced by the CRISPR/Cas9
788 transfection. All four examples show a range of insertion, deletion or mismatch mutations boxed
789 in red. The "+2 insertion" with a dotted light green box highlights two alanine insertions near the
790 target site. The "-6 deletion" highlights six absent base pairs with a light blue box which include
791 the target site. **c**, The mutation rates were calculated at each time point from Δ*Ov-grn-1 in vitro*
792 cultured adult flukes with qPCR and the averages and standard deviation were determined . RT-
793 qPCR electrophoresis gel (lower image) shows *Ov-grn-1* RNA levels are reduced in Δ*Ov-grn-1*
794 adult flukes.
795
796 **Supplementary Figure 2. Extended image set showing Δ*Ov-grn-1* adult fluke ES products**
797 **induce less *in vitro* cell proliferation and wound repair.** **a**, Representative cell proliferation
798 images of H69 immortalized human cholangiocyte cell line co-cultured with flukes in Trans-well
799 plates; shown at 24 and 72hrs. **b**, Comparing the difference in cell proliferation values from Fig.
800 2b between ES products from the *ΔOv-grn-1* flukes and ES from WT flukes revealed a linear
801 correlation of reduction of cell proliferation that increases over time. **c**, Representative image of
802 scratch wound repair of cultured cholangiocytes when H69 cells were co-cultured in Trans-well
803 plates with flukes; time points from 0 - 36 hours post-scratch. Dotted line indicates the margin of
804 the wound. **d**, Scratch wound repair assay quantified values from Fig. 2d showed an increasing
805 linear correlation over time of reduced wound closure when plotting the difference between the
806 Δ*Ov-grn-1* and the WT fluke groups. Panels **b** and **d**: mean ± SD, three biological replicates.
807
808 **Supplementary Figure 3. CRISPR/Cas9 ineffective at silencing gene expression in**
809 **metacercariae (MC).** Expression of *Ov-grn-1* mRNA in wild type (WT), mock-transfected, and
810 Δ*Ov-grn-1* MC over five days as quantified with qPCR and plotted relative to the WT untreated
811 group; mean ± SD from three replicates. ****$P<0.0001$; Δ*Ov-grn-1* compared to WT control
812 group, $P>0.05$; non-significant (ns) difference seen between mock (control) group using the
813 two-way ANOVA Holm-Sidak multiple comparison test.
814
815 **Supplementary Figure 4. Representative wide-angle view of anti-ACTA2**
816 **immunofluorescence and bright field liver sections.** Thin liver sections presented in bright
817 field or under fluorescent light following probing with anti-ACTA2 antibody; fluorescence
818 intensity shown on a blue/green/red scale. These images were used to create the bright
819 field/immunofluorescence overlay and zoomed images in Fig. 4d.
820
821
822
823
824

825
826 **References**
827

828 1. B. Sripa *et al.*, Opisthorchiasis and Opisthorchis-associated cholangiocarcinoma in
829 Thailand and Laos. *Acta Trop* **120 Suppl 1**, S158-168 (2011).
830 2. J. S. Pagano *et al.*, Infectious agents and cancer: criteria for a causal relation. *Semin*
831 *Cancer Biol* **14**, 453-471 (2004).
832 3. T. Laha *et al.*, Gene discovery for the carcinogenic human liver fluke, Opisthorchis
833 viverrini. *BMC genomics* **8**, 189 (2007).
834 4. N. Khuntikeo *et al.*, Cohort profile: cholangiocarcinoma screening and care program
835 (CASCAP). *BMC Cancer* **15**, 459 (2015).
836 5. N. Khuntikeo, W. Loilome, B. Thinkhamrop, N. Chamadol, P. Yongvanit, A
837 Comprehensive Public Health Conceptual Framework and Strategy to Effectively
838 Combat Cholangiocarcinoma in Thailand. *PLoS Negl Trop Dis* **10**, e0004293 (2016).
839 6. P. J. Brindley, A. Loukas, Helminth infection-induced malignancy. *PLoS Pathog* **13**,
840 e1006393 (2017).
841 7. A. Papatpremsiri *et al.*, Suppression of Ov-grn-1 encoding granulin of Opisthorchis
842 viverrini inhibits proliferation of biliary epithelial cells. *Exp Parasitol* **148**, 17-23 (2015).
843 8. M. J. Smout *et al.*, Carcinogenic Parasite Secretes Growth Factor That Accelerates
844 Wound Healing and Potentially Promotes Neoplasia. *PLoS Pathog* **11**, (2015).
845 9. K. F. Hoffmann, P. J. Brindley, M. Berriman, Medicine. Halting harmful helminths.
846 *Science* **346**, 168-169 (2014).
847 10. P. D. Hsu, E. S. Lander, F. Zhang, Development and applications of CRISPR-Cas9 for
848 genome engineering. *Cell* **157**, 1262-1278 (2014).
849 11. J. D. Sander, J. K. Joung, CRISPR-Cas systems for editing, regulating and targeting
850 genomes. *Nat Biotechnol* **32**, 347-355 (2014).
851 12. S. Waaijers, M. Boxem, Engineering the Caenorhabditis elegans genome with
852 CRISPR/Cas9. *Methods* **68**, 381-388 (2014).
853 13. J. B. Lok, H. Shao, H. C. Massey, X. Li, Transgenesis in Strongyloides and related
854 parasitic nematodes: historical perspectives, current functional genomic applications and
855 progress towards gene disruption and editing. *Parasitology* **144**, 327-342 (2017).
856 14. S. S. Gang *et al.*, Targeted mutagenesis in a human-parasitic nematode. *PLoS Pathog* **13**,
857 e1006675 (2017).
858 15. N. D. Young *et al.*, The Opisthorchis viverrini genome provides insights into life in the
859 bile duct. *Nat Commun* **5**, 4378 (2014).
860 16. A. N. Shah, C. F. Davey, A. C. Whitebirch, A. C. Miller, C. B. Moens, Rapid reverse
861 genetic screening using CRISPR in zebrafish. *Nat Methods* **12**, 535-540 (2015).
862 17. C. Yu, Y. Zhang, S. Yao, Y. Wei, A PCR based protocol for detecting indel mutations
863 induced by TALENs and CRISPR/Cas9 in zebrafish. *PLoS One* **9**, e98282 (2014).
864 18. M. C. Canver *et al.*, Integrated design, execution, and analysis of arrayed and pooled
865 CRISPR genome-editing experiments. *Nat Protoc* **13**, 946-986 (2018).
866 19. L. Pinello *et al.*, Analyzing CRISPR genome-editing experiments with CRISPResso. *Nat*
867 *Biotechnol* **34**, 695-697 (2016).
868 20. M. Guido, M. Rugge, G. Leandro, I. M. Fiel, S. N. Thung, Hepatic stellate cell
869 immunodetection and cirrhotic evolution of viral hepatitis in liver allografts. *Hepatology*
870 **26**, 310-314 (1997).

871 21. P. Sithithaworn, V. Pipitgool, T. Srisawangwong, D. B. Elkins, M. R. Haswell-Elkins,
872 Seasonal variation of Opisthorchis viverrini infection in cyprinoid fish in north-east
873 Thailand: implications for parasite control and food safety. *Bull World Health Organ* **75**,
874 125-131 (1997).
875 22. A. Papatpremsiri, Effect of radiation attenuation of metacercariae and gene silencing
876 targeting granulin on infection with Opisthorchis viverrini, Doctor of Philosophy in
877 biomedical science, Khon Kaen University, Thailand, (2014).
878 23. B. Sripa, S. Kaewkes, Gall bladder and extrahepatic bile duct changes in Opisthorchis
879 viverrini-infected hamsters. *Acta Tropica* **83**, 29-36 (2002).
880 24. S. Piratae *et al.*, Molecular characterization of a tetraspanin from the human liver fluke,
881 Opisthorchis viverrini. *PLoS Negl Trop Dis* **6**, e1939 (2012).
882 25. H. Yang, J. J. Wu, T. Tang, K. D. Liu, C. Dai, CRISPR/Cas9-mediated genome editing
883 efficiently creates specific mutations at multiple loci using one sgRNA in Brassica napus.
884 *Sci Rep* **7**, 7489 (2017).
885 26. S. N. Chan, N. Abu Bakar, M. Mahmood, C. L. Ho, N. A. Shaharuddin, Molecular
886 cloning and characterization of novel phytocystatin gene from turmeric, Curcuma longa.
887 *Biomed Res Int* **2014**, 973790 (2014).
888 27. H. Chen, M. Rangasamy, S. Y. Tan, H. Wang, B. D. Siegfried, Evaluation of five
889 methods for total DNA extraction from western corn rootworm beetles. *PLoS One* **5**,
890 e11963 (2010).
891 28. J. J. Vasquez, C. Wedel, R. O. Cosentino, T. N. Siegel, Exploiting CRISPR-Cas9
892 technology to investigate individual histone modifications. *Nucleic Acids Res*, (2018).
893 29. T. D. Schmittgen, K. J. Livak, Analyzing real-time PCR data by the comparative C(T)
894 method. *Nat Protoc* **3**, 1101-1108 (2008).
895 30. O. Strannegard, A. Yurchision, Formation of rabbit reaginic antibodies to protein and
896 hapten-protein conjugates. *Immunology* **16**, 387-397 (1969).
897 31. S. Chaiyadet *et al.*, Suppression of mRNAs encoding CD63 family tetraspanins from the
898 carcinogenic liver fluke Opisthorchis viverrini results in distinct tegument phenotypes.
899 *Sci Rep* **7**, 14342 (2017).
900 32. M. F. Sentmanat, S. T. Peters, C. P. Florian, J. P. Connelly, S. M. Pruett-Miller, A Survey
901 of Validation Strategies for CRISPR-Cas9 Editing. *Sci Rep* **8**, 888 (2018).
902 33. K. Ninlawan *et al.*, Opisthorchis viverrini excretory/secretory products induce toll-like
903 receptor 4 upregulation and production of interleukin 6 and 8 in cholangiocyte. *Parasitol*
904 *Int* **59**, 616-621 (2010).
905 34. R. J. Tynan *et al.*, A comparative examination of the anti-inflammatory effects of SSRI
906 and SNRI antidepressants on LPS stimulated microglia. *Brain Behav Immun* **26**, 469-479
907 (2012).
908 35. C. C. Liang, A. Y. Park, J. L. Guan, In vitro scratch assay: a convenient and inexpensive
909 method for analysis of cell migration in vitro. *Nat Protoc* **2**, 329-333 (2007).
910 36. M. J. Smout *et al.*, Infection with the carcinogenic human liver fluke, Opisthorchis
911 viverrini. *Mol Biosyst* **7**, 1367-1375 (2011).
912 37. M. A. Pereira, Tratamento com células derivadas do fígado embrionário retarda a
913 progressão da fibrose hepática em ratos, Tese de Doutorado, Universidade de São Paulo,
914 Brazil, (2016).
915

Figure 1

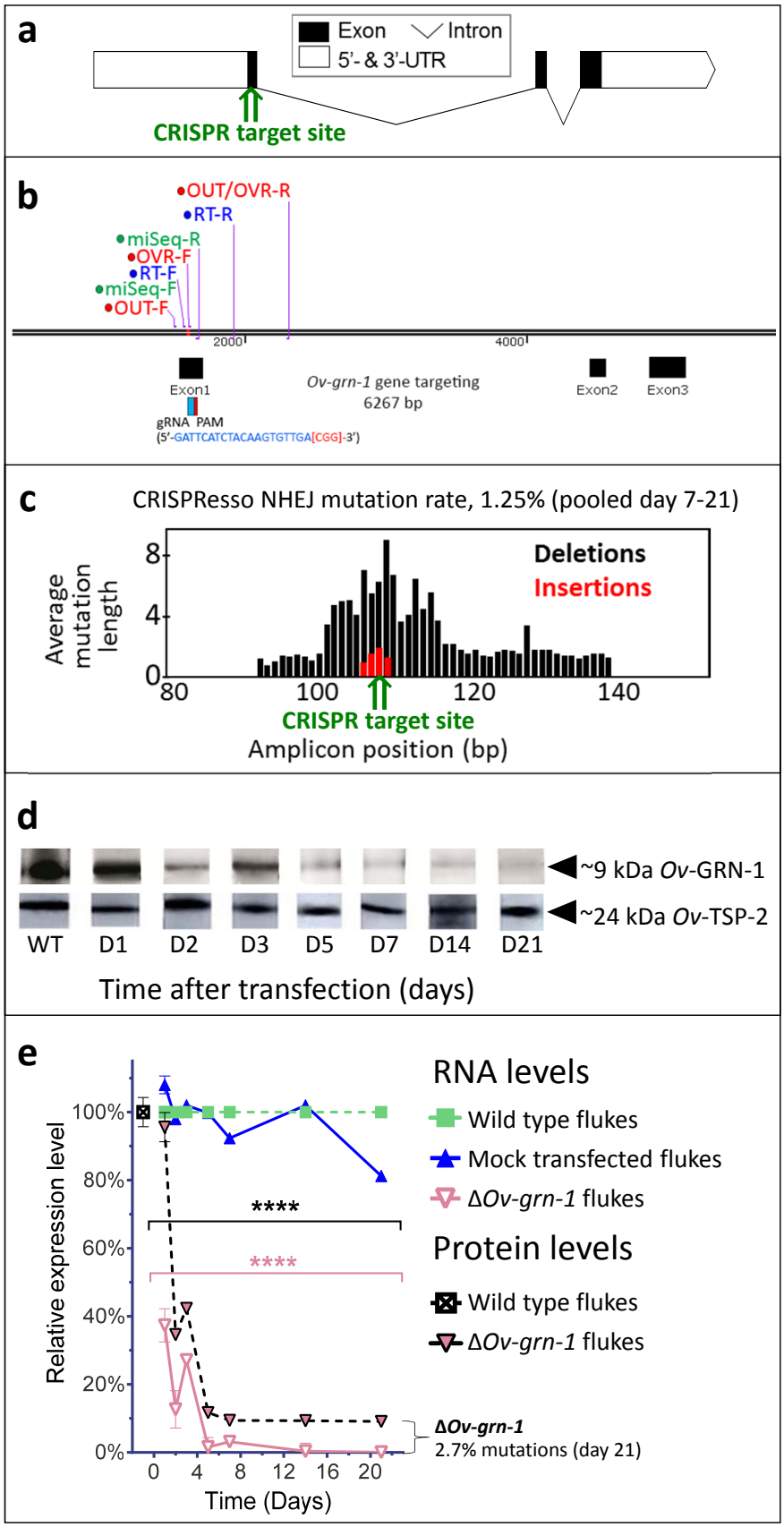
a
Exon
Intron
5'- & 3'-UTR
CRISPR target site
b
OUT/OVR-R
RT-R
miSeq-R
OVR-F
RT-F
miSeq-F
OUT-F
2000
4000
Exon1
Ov-grn-1 gene targeting
6267 bp
Exon2
Exon3
gRNA PAM
(5'-GATTCATCTACAAGTGTTGA[CGG]-3')
c
CRISPResso NHEJ mutation rate, 1.25% (pooled day 7-21)
Average mutation length
Deletions
Insertions
CRISPR target site
Amplicon position (bp)
d
~9 kDa Ov-GRN-1
~24 kDa Ov-TSP-2
WT
D1
D2
D3
D5
D7
D14
D21
Time after transfection (days)
e
Relative expression level
Time (Days)
RNA levels
Wild type flukes
Mock transfected flukes
ΔOv-grn-1 flukes
Protein levels
Wild type flukes
ΔOv-grn-1 flukes
****
****
ΔOv-grn-1
2.7% mutations (day 21)

Figure 2

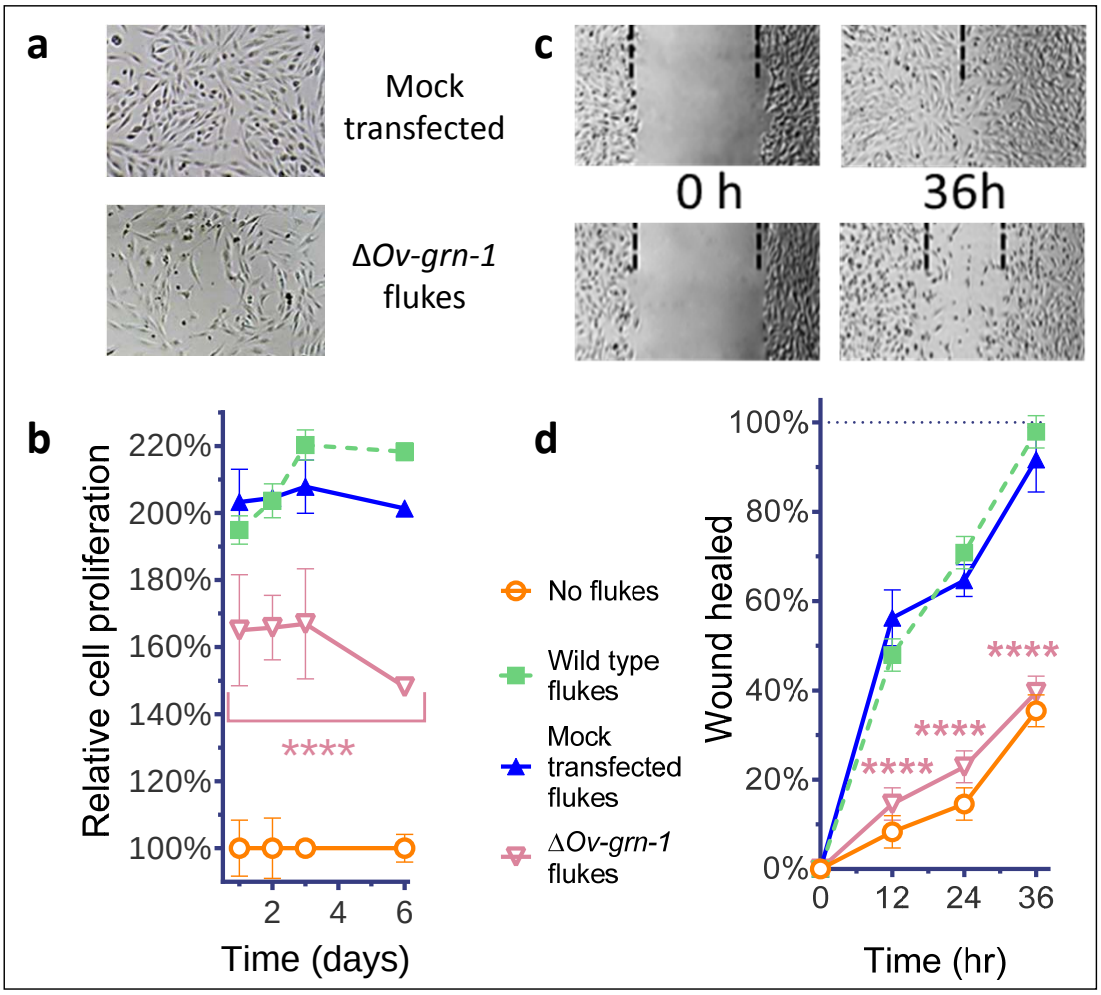
a
Mock transfected
ΔOv-grn-1 flukes
c
0 h
36h
b
Relative cell proliferation
220%
200%
180%
160%
140%
120%
100%
****
2
4
6
Time (days)
d
No flukes
Wild type flukes
Mock transfected flukes
ΔOv-grn-1 flukes
Wound healed
100%
80%
60%
40%
20%
0%
****
****
****
0
12
24
36
Time (hr)

Figure 3

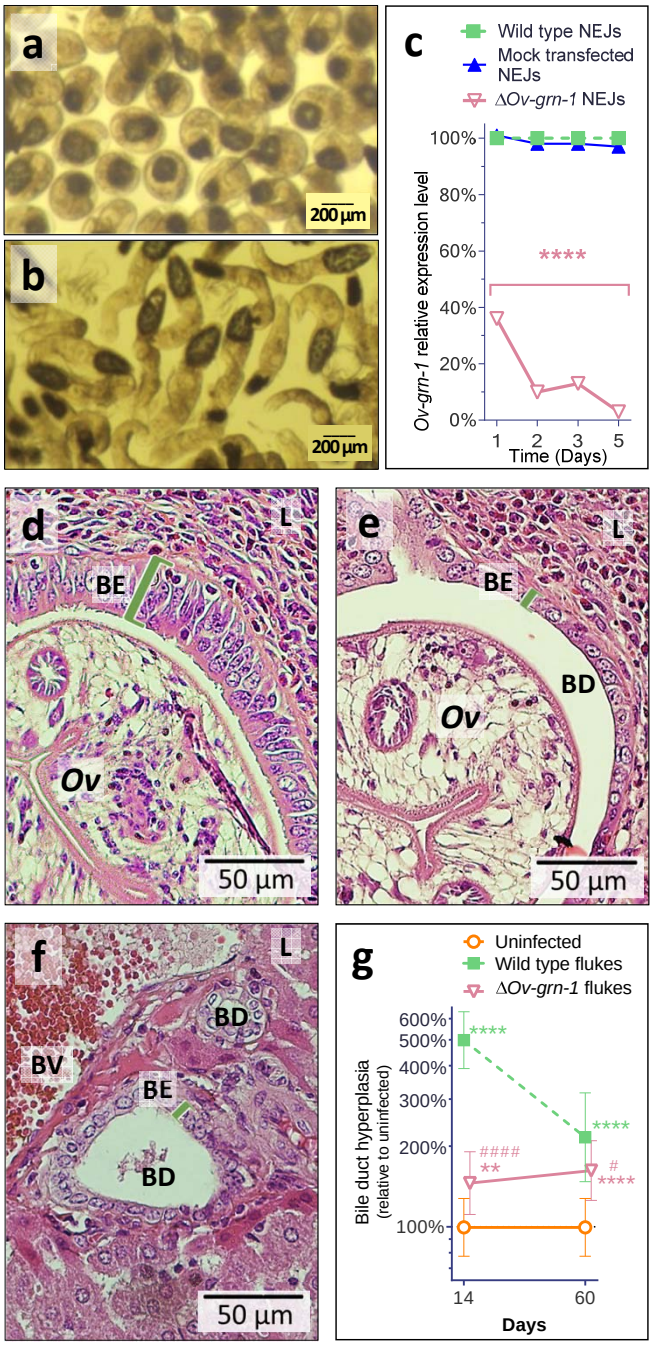
a
200 µm
b
200 µm
c
Wild type NEJs
Mock transfected NEJs
ΔOv-grn-1 NEJs
Ov-grn-1 relative expression level
100%
80%
60%
40%
20%
0%
****
1
2
3
5
Time (Days)
d
L
BE
Ov
50 µm
e
L
BE
BD
Ov
50 µm
f
L
BD
BV
BE
BD
50 µm
g
Uninfected
Wild type flukes
ΔOv-grn-1 flukes
Bile duct hyperplasia (relative to uninfected)
600%
500%
400%
300%
200%
100%
****
****
####
**
#
****
14
60
Days

Figure 4

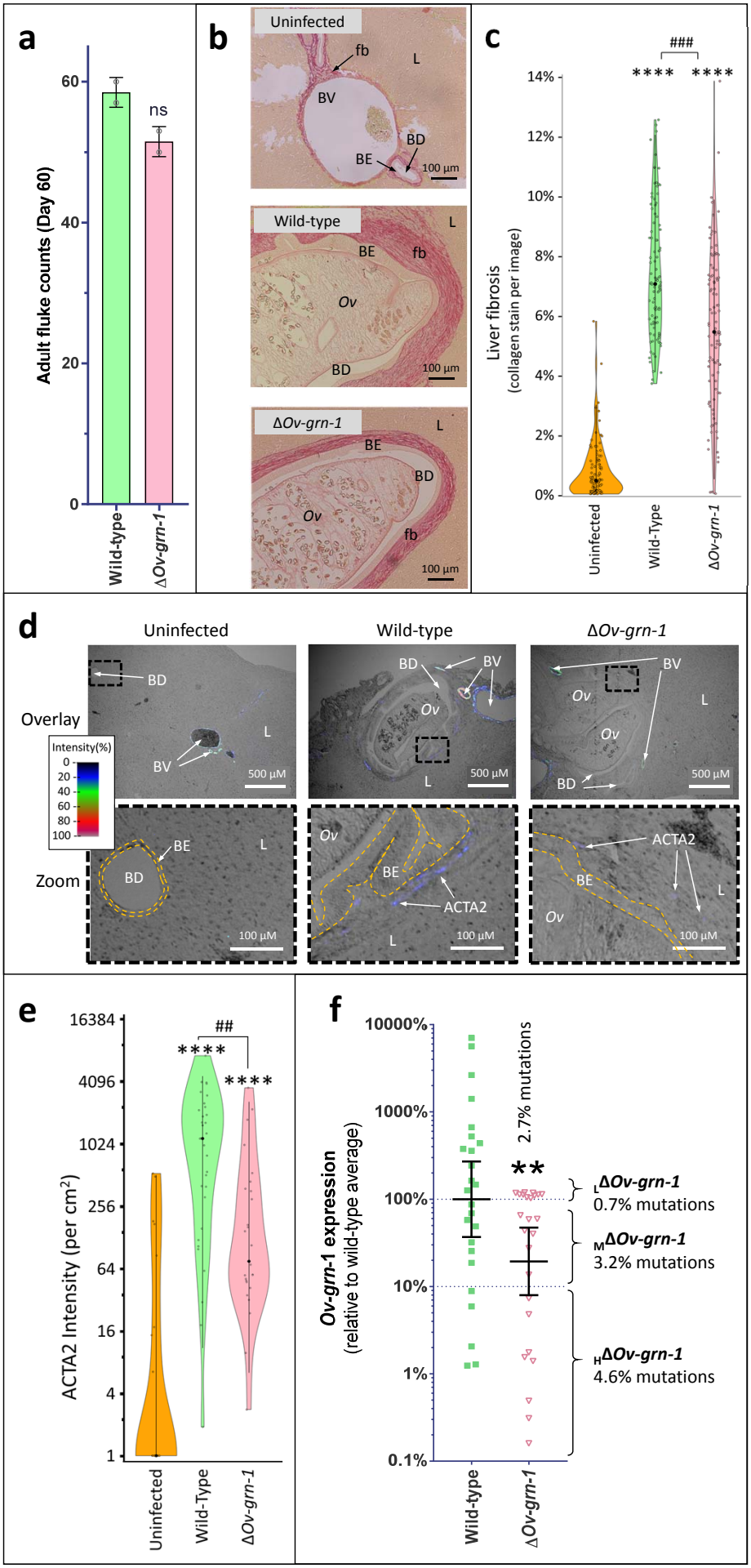
a
Adult fluke counts (Day 60)
60
40
20
0
ns
Wild-type
ΔOv-grn-1
b
Uninfected
fb
L
BV
BD
BE
100 µm
Wild-type
BE
fb
Ov
BD
ΔOv-grn-1
c
Liver fibrosis
(collagen stain per image)
14%
12%
10%
8%
6%
4%
2%
0%
###
****
Uninfected
Wild-Type
ΔOv-grn-1
d
Uninfected
Wild-type
ΔOv-grn-1
Overlay
Intensity(%)
Zoom
500 µM
100 µM
ACTA2
e
ACTA2 Intensity (per cm²)
16384
4096
1024
256
64
16
4
1
##
****
Uninfected
Wild-Type
ΔOv-grn-1
f
Ov-grn-1 expression
(relative to wild-type average)
10000%
1000%
100%
10%
1%
0.1%
2.7% mutations
**
LΔOv-grn-1
0.7% mutations
MΔOv-grn-1
3.2% mutations
HΔOv-grn-1
4.6% mutations
Wild-type
ΔOv-grn-1

Supplementary Figure S1

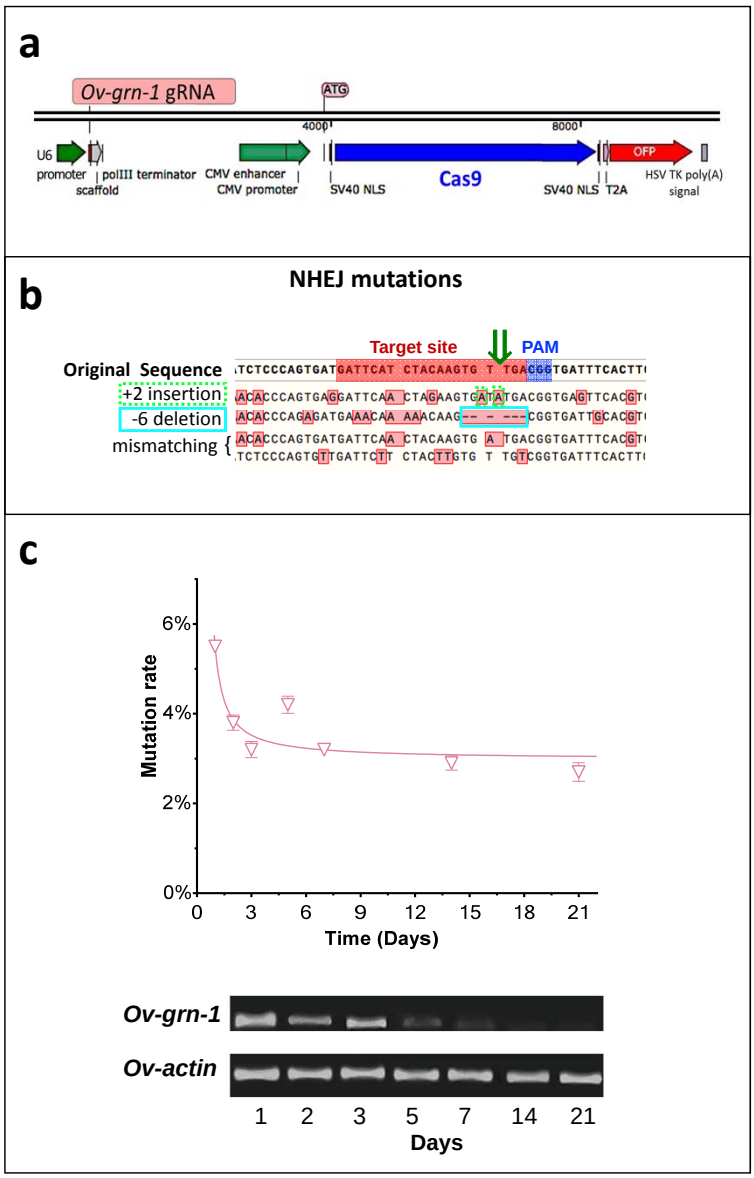

Supplementary Figure S2

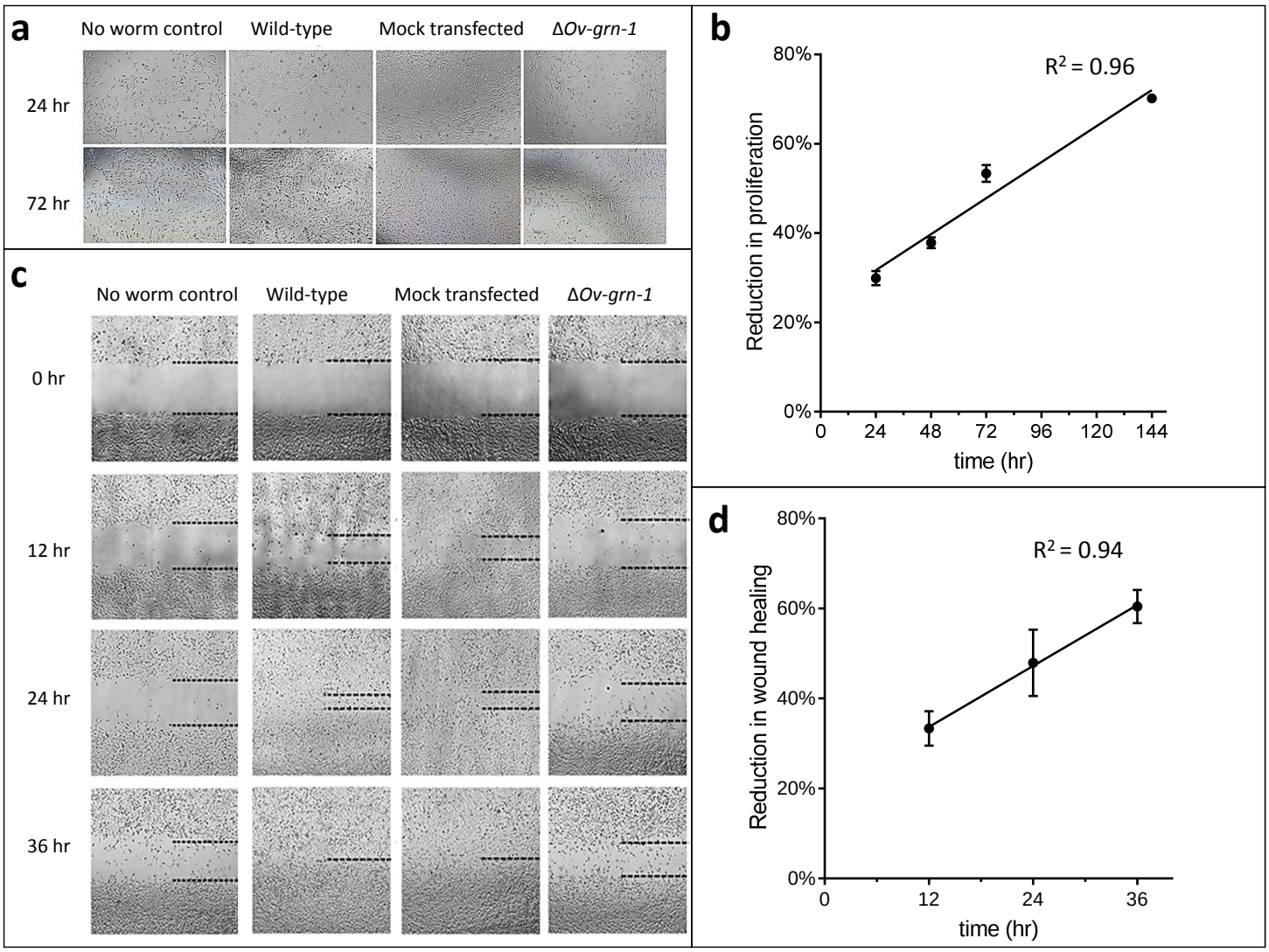

Supplementary Figure S3

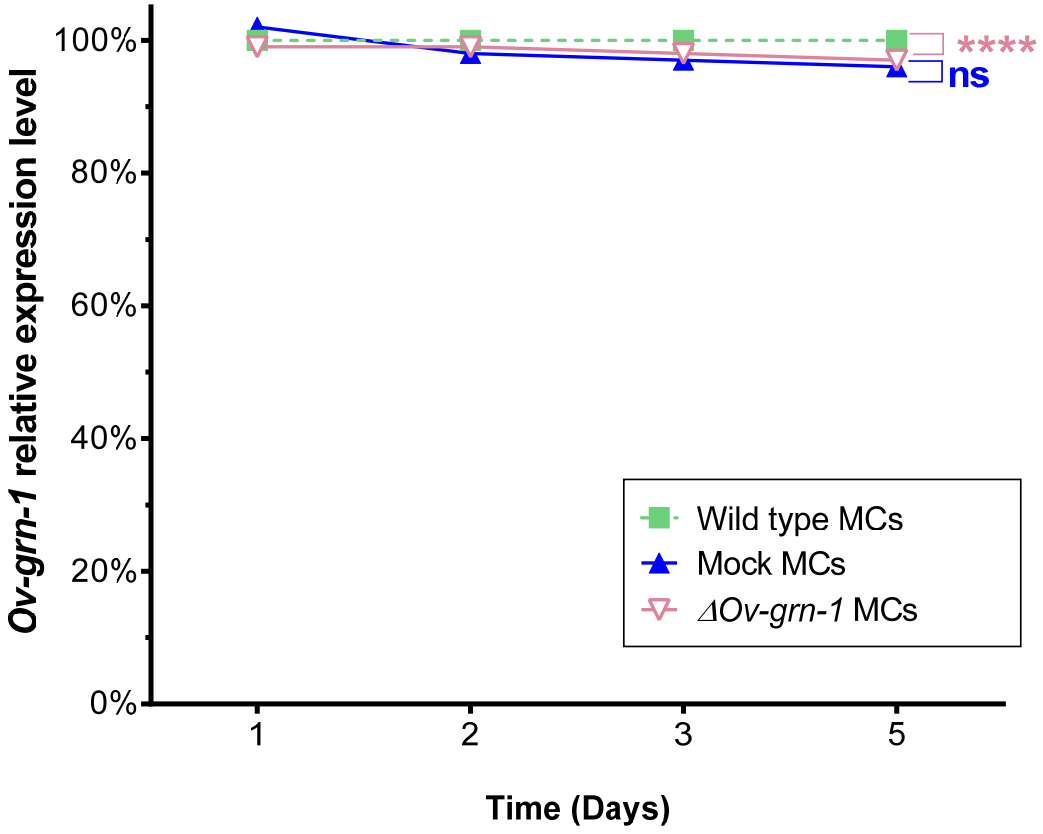
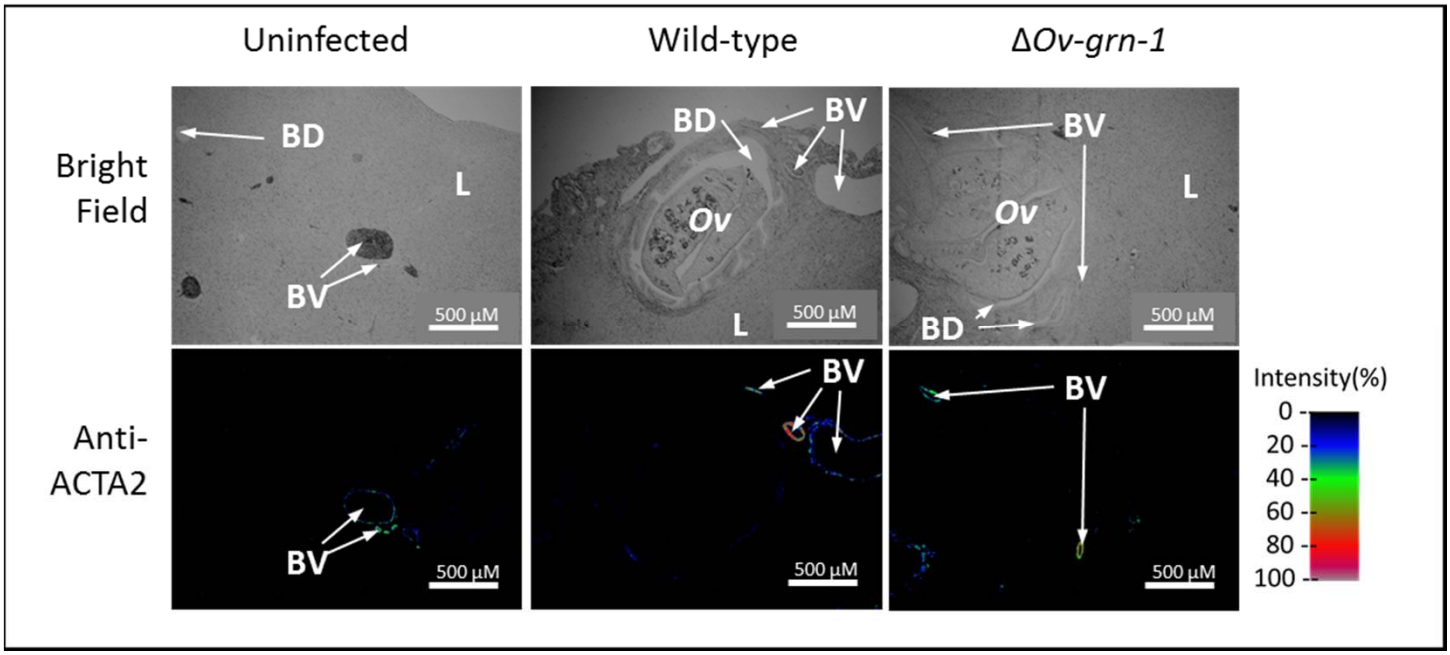
Supplementary Figure S4